Eikonal-based initiation of fibrillatory activity in thin-walled cardiac propagation models

Antoine Herlin and Vincent Jacquemet

Institut de Génie Biomédical, Department of Physiology,

Faculty of Medicine, Université de Montréal, Montréal, Canada;

Centre de recherche, Hôpital du Sacré-Coeur de Montréal.

Published in Chaos (2011),vol. 21, pp. 043136

Abstract

Reentrant arrhythmias can be simulated in electrophysiological models of electrical impulse propagation governed by a reaction-diffusion system. To facilitate the initiation of a large number of independent episodes of simulated arrhythmias with controllable level of complexity, a new approach is proposed for thin-walled geometries in which depolarization wave dynamics is essentially two-dimensional. Points representing phase singularities are first randomly distributed over the epicardial surface and are assigned a topological charge (direction of rotation). A qualitatively-correct phase map is then reconstructed on the whole surface by interpolation. The eikonal-diffusion equation is used to iteratively regularize the phase map based on a priori information on wavefront propagation. An initial condition for the reaction-diffusion model is created from the resulting phase map with multiple functional/anatomical reentries. Results in an atrial model demonstrate the ability to generate statistical realizations of the same dynamics and to vary the level of complexity measured by the number of phase singularities. A library of 100 simulations with an average number of phase singularities ranging from 1 to 10 is created. An extension to volumetric patient-specific atrial models including fiber orientation and a fast conducting system is presented to illustrate possible applications.

Lead paragraph

Atrial fibrillation (AF) is the most frequent rhythm disorder in humans. It often leads to severe complications such as heart failure and stroke. AF affects the electrical activity of the upper chambers of the heart (the atria). Computer models of the atria have been developed to describe the propagation of electrical excitation waves in the heart muscle using nonlinear partial differential equations of the reaction-diffusion type. These models have contributed to the understanding of AF by isolating and illustrating different mechanisms of AF and by investigating the arrhythmogenic processes in controlled setups. Reentry (single or multiple self-sustained activation waves) was found to be a key element in these mechanisms. In order to test a therapeutical intervention, a diagnosis technique or a signal processing tool in an atrial model, many different, independent episodes of simulated AF have to be initiated. We propose a new approach for simulated AF initiation in which a randomly-generated but plausible initial condition is generated using *a priori* knowledge about wavefront propagation. The complexity of the dynamics measured as the number of

phase singularities can be controlled. This allows the creation of a database of simulated AF episodes with varying degrees of complexity.

I. INTRODUCTION

A key advantage of computer modeling is the ability to study the effect of changing only one parameter, the remaining parameters being kept identical. In the context of reaction-diffusion anatomical models of AF, this paper presents a new computational framework to change and control the complexity of simulated AF dynamics without altering the underlying tissue substrate, and to simulate a similar AF dynamics in a different atrial geometry.

Most previous simulation studies used programmed stimulation protocols to initiate AF, including S_1–S_2 stimulation [27, 30–33], cross-shock stimulation [17, 18], or train of ectopic foci at different locations [9, 10]. Narrow vulnerability windows often made the initiation protocols time-consuming. Repeating the simulations in another atrial geometry (which is increasingly common as patient-specific models are being developed [19]) usually required restarting the initiation protocols from scratch.

These initiation protocols attempted to reproduce the physiological conditions and mechanisms leading to the onset of AF. When a biophysical modeling approach is applied to evaluate a pharmacological [17] or electrophysiological therapy [6, 27], electrogram [15, 34] or ECG signal processing tools [20, 21], however, the precise conditions giving rise to the first AF episode are not necessarily needed, or, as often in clinical studies, not available. These simulation studies require a larger number of independent AF episodes either to compute electrical signals or as initial condition before an intervention is performed.

A method to generate a library of simulated AF episodes consists in extracting different states in the course of a long simulation (up to several minutes) [28], assuming a high sensitivity to initial conditions. This approach becomes inappropriate for organized types of AF (e.g. focal AF). An alternative technique, also designed for turbulent dynamics, is to randomly perturb the membrane potential field of a fibrillatory initial condition [26]. In the case of initiation of anatomical macroreentry, the use of activation maps computed from the eikonal-diffusion equation was proved to be a valuable tool [12, 13].

This paper extends the eikonal approach to handle cases with multiple reentries by randomly distributing phase singularities on the atrial surface and constructing an initial con-

dition with the same set of phase singularities. Test cases include a simplified atrial model, patient-specific models of the left atrium and a more sophisticated volumetric model of the atria. The results demonstrate the ability to generate a database of simulated AF episodes with a broad range of average number of wavelets and phase singularities.

II. METHODS

A. Cardiac propagation model

The propagation of the cardiac impulse in the myocardium can be described by the evolution of the membrane potential field $V_m(\mathbf{x}, t)$. According to the monodomain theory, this evolution is governed by a reaction-diffusion equation [25]:

$$C_m \frac{\partial V_m}{\partial t} = \beta^{-1} \nabla \cdot \boldsymbol{\sigma} \nabla V_m - I_{\text{ion}} \ , \tag{1}$$

where C_m is the membrane capacitance per unit area of membrane, β is the area of membrane per unit volume, and $\boldsymbol{\sigma}$ is the (effective) conductivity tensor. The ionic current I_{ion} depends on V_m and on internal variables $\mathbf{s}$ (intracellular ionic concentrations and channel gate states) that satisfy a system of ordinary differential equations $\mathrm{d}\mathbf{s}/\mathrm{d}t = F_{\mathbf{s}}(V_m, \mathbf{s})$. No-flux boundary condition is assumed, i.e. $\mathbf{n} \cdot \boldsymbol{\sigma} \nabla V_m = 0$ where $\mathbf{n}$ is the unit vector normal to the boundary. An initial condition $V_m(\mathbf{x}, 0) = V_0(\mathbf{x})$ and $\mathbf{s}(\mathbf{x}, 0) = \mathbf{s}_0(\mathbf{x})$ has to be specified.

In this paper, the ionic current I_{ion} is described by the Courtemanche *et al.* model [4]. To reproduce ion channel remodeling induced by chronic atrial fibrillation [22], channel maximum conductances are modified. Similarly to Kharche *et al.* [16], the L-type Ca^{2+} current (I_{CaL}) is reduced by 63% and the transient outward K^+ current (I_{to}) by 65% (data from human chronic AF atrial cells measured by whole cell patch clamp [35]). The inward rectifier K^+ current (I_{K1}) is increased by 73% (measurement near the resting potential in chronic AF patients [8]). As a result of these modifications, the action potential is triangular-shaped and the effective refractory period at 60 bpm is about 160 ms.

Equation (1) is solved numerically on three-dimensional cubic grids using finite difference discretization [1] ($\Delta x = 330$ μm) and explicit time integration ($\Delta t = 20$ μs). During the simulations, membrane potentials at each node of a triangulated surface mesh representing the epicardium are stored for subsequent analysis (Subsect. II G). This triangular mesh will also be used for the construction of the initial conditions (Subsect. II F).

B. Identification of phase singularities

Phase singularity (PS) analysis provides a tool to quantify the complex spatio-temporal behavior observed in computer models or animal models of cardiac arrhythmia [2, 11]. It enables to count the number of simultaneous wavelets and identify the location of arrhythmogenic regions associated with reentries or wavebreaks. During a reentrant activation, a PS is typically located at the center of the rotating wave or at the pivot point of a U-turn. When the membrane potential field $V_m(\mathbf{x}, t)$ is known, the phase field θ can be defined as:

$$\theta(\mathbf{x}, t) = \mathrm{atan2}\big(V_m(\mathbf{x}, t + \tau_{\mathrm{delay}}) - V^*,\ V_m(\mathbf{x}, t) - V^*\big)\ , \tag{2}$$

where atan2 is the four-quadrant inverse tangent, τ_{delay} is the time delay for phase space reconstruction and (V^*, V^*) is the chosen origin of the phase space [11]. For the membrane model used here, we chose $\tau_{\mathrm{delay}} = 5$ ms and $V^* = -55$ mV based on previous works [11].

Since only thin-walled three-dimensional atrial models are considered here, the electrical activity will be analyzed through its manifestation on the epicardial surface (outer surface of the atria), like in most experimental optical mapping setups. This assumes that the membrane potential field is approximately uniform in the thickness direction. In these two-dimensional cases, the topological charge q of a domain delimited by a closed curve Γ is defined as the contour integral [7]

$$q(\Gamma) = \frac{1}{2\pi} \oint_{\Gamma} \nabla\theta \cdot \mathrm{d}\boldsymbol{\ell}\ , \tag{3}$$

which gives an integer. The gradient takes into account the angular nature of θ (θ is defined modulo 2π). When Γ encircles a discontinuity point, a nonzero value for q may be obtained (typically ± 1). This situation corresponds to a PS. The sign is associated with the direction of rotation of the reentrant activity (chirality). When Γ encircles an anatomical obstacle (or hole), a nonzero value corresponds to a reentry anchored around the obstacle [7]. This case will however not be counted as a PS.

Phase singularity location can be identified and tracked by successive application of this formula (for example on every triangle of a triangulated surface) [11]. The state at a given time can therefore be qualitatively described by the number n of PS, by their location $\mathbf{x}_i$ and their topological charge q_i. The question arises whether it is possible to construct a tissue state with n PS with given locations and topological charges. The next subsections address this problem and its application to the initiation of fibrillatory activity.

C. Random distribution of phase singularities

The objective is to distribute n points on a coarse triangulated surface (N = 800–2,000 nodes) and assign their topological charge ± 1. We aim at generating PS configurations in which PS are not too close to each other and two neighboring PS have preferably opposite charge. For each configuration $\{\mathbf{x}_i, q_i\}$, the minimum distance d and the energy E are defined as:

$$d(\{\mathbf{x}_i\}) = \min_{i \neq j} \ \mathrm{dist}(\mathbf{x}_i, \mathbf{x}_j) \tag{4}$$

$$E(\{\mathbf{x}_i, q_i\}) = \sum_{i \neq j} \frac{q_i \, q_j}{\mathrm{dist}(\mathbf{x}_i, \mathbf{x}_j)} \ . \tag{5}$$

The idea is to maximize d while minimizing E. The distance $\mathrm{dist}(\mathbf{x}, \mathbf{y})$ is the length of the shortest path between $\mathbf{x}$ and $\mathbf{y}$ on the surface [5]. The distance matrix (all-pairs shortest path) is computed using Johnson's algorithm [3] as implemented by David Gleich in the toolbox MatlabBGL (available at Matlab Central file exchange).

First, a point $\mathbf{x}_1$ is randomly selected. The optimum minimum distance $d_{\mathrm{opt}}(\mathbf{x}_1, n)$ is estimated by taking the maximum of $d(\{\mathbf{x}_i\})$ with $\mathbf{x}_1$ fixed over 1,000 random selections of the $n-1$ remaining points. For small values of n, $d_{\mathrm{opt}}(\mathbf{x}_1, n)$ depends on $\mathbf{x}_1$. Then, sets of $n-1$ points are randomly selected until $d(\{\mathbf{x}_i\}) > (1 - \epsilon_d) \, d_{\mathrm{opt}}(\mathbf{x}_1, n)$ where ϵ_d lies in the range 0.1 to 0.2. This ensures that the points are well spread over the surface.

The topological charges are obtained by minimizing the energy, the positions $\{\mathbf{x}_i\}$ being fixed. The first value q_1 is randomly set to ± 1. The energy is computed for all configurations of the remaining $n-1$ points satisfying the constraint $\sum_i q_i = 0$ if n is even and $|\sum_i q_i| = 1$ if n is odd. The configuration with minimal energy is selected. Typically, the two nearest PS will have opposite topological charge.

D. Phase field reconstruction

Interpolation of the phase field $\theta(\mathbf{x})$ from phase singularity configuration $\{\mathbf{x}_i, q_i\}$ is performed on an oriented triangular mesh of intermediate resolution (N = 11,000 to 17,000 nodes; $\Delta x \approx 1$ mm). The small circuit formed by the triangles surrounding the point $\mathbf{x}_i$ is denoted by Γ_i. Its orientation follows that of the surrounding triangles and its length L_i is of the order of 6 mm. To avoid a phase unwrapping problem, the complex phase field

$\phi = \exp(\mathrm{i}\theta)$ is used [12] (the non-italic i denotes the imaginary unit). Its value is set to $\phi = \exp(\mathrm{i}q_i\ell/L_i)$ on Γ_i, where ℓ is the curvilinear coordinate along the oriented curve Γ_i (the origin of curvilinear coordinate is chosen arbitrarily). Interpolation in the entire domain is obtained by solving the Laplace equation $\Delta\phi = 0$ with no-flux boundary condition where no value is assigned to ϕ (e.g. veins or valves) [23]. Then $\phi_0 = \phi/|\phi|$ provides an estimate of the desired complex phase field. Indeed, by construction, $\theta_0 = \arg\phi_0$ has a PS at $\mathbf{x}_i$ with topological charge q_i for each i. However, ϕ may have one or more zeros. This results in the creation of additional PS at these points.

The local wavelength of a phase field can be defined as:

$$\lambda(\mathbf{x}) = 2\pi \, \|\nabla\theta\|^{-1} = 2\pi \, \|\nabla\phi\|^{-1} \; . \tag{6}$$

For a reentry with period T, this local wavelength is related to the conduction velocity (CV in cm/s) by the formula $\lambda = CV \cdot T$ [12]. The local wavelength for ϕ_0 is typically very non-uniform, especially when n is small. As a result, the phase field provides an inaccurate representation of a reentrant activation pattern. In order to iteratively regularize the phase field using *a priori* information about wavefront propagation, the eikonal-diffusion equation will be applied as a filter. The complex form of this equation reads $\mathcal{F}[\phi] = 0$, where the functional $\mathcal{F}$ is defined as [12]

$$\mathcal{F}[\phi] = c \, \|\nabla\phi\| - D \, \mathrm{Im} \, \nabla \cdot (\phi^* \nabla\phi) - 1 \; . \tag{7}$$

The parameter c is the scaled conduction velocity (in cm/rad) and D is a diffusion coefficient (in cm^2). When D tends to zero, the equation $\mathcal{F}[\phi] = 0$ becomes $\lambda(\mathbf{x}) = 2\pi c = \text{const}$. This suggests that reducing the values of $|\mathcal{F}|$ would regularize the spatial distribution of wavelength and conduction velocity. A Newton-based iterative scheme has been proposed to solve this equation [12, 13]. Briefly, an approximate solution ϕ to $\mathcal{F}[\phi] = 0$ can be improved by applying a phase correction $\phi \mapsto \phi \exp(\mathrm{i}\Psi)$. The correction Ψ is the solution to the Newton's method update equation generalized to functionals [12]:

$$\mathcal{F}[\phi] + \frac{\mathrm{d}}{\mathrm{d}\epsilon} \mathcal{F}[\phi \exp(\mathrm{i}\epsilon\Psi)] \bigg|_{\epsilon=0} = 0 \; . \tag{8}$$

After substituting Eq. (7) into Eq. (8), this relation becomes a steady-state convection-diffusion equation in Ψ:

$$c \, \frac{\mathrm{Im} \; \phi \, \nabla\phi^*}{\|\nabla\phi\|} \, \nabla\Psi + D\Delta\Psi = c \, \|\nabla\phi\| - 1 - D \, \mathrm{Im} \, \nabla \cdot (\phi^* \nabla\phi) \; , \tag{9}$$

with Dirichlet boundary condition on each of the circuits Γ_i and no-flux boundary condition everywhere else. Spatial discretization of this equation is performed through a dedicated finite element method published previously [13]. Practically, the iterations start with ϕ_0 obtained from Laplacian interpolation (see beginning of Subsect. II D). At step k, a phase correction $\phi_{k+1} = \phi_k \exp(\mathrm{i}\Psi)$ is applied (so $|\phi_k| = 1$ always holds), where Ψ is the solution to Eq. (9) with $\phi = \phi_k$.

The update equation (9) can be interpreted the following way in the low-diffusion limit. With $\phi = \exp(\mathrm{i}\theta_k)$ and $D = 0$, Eq. (9) can be written as:

$$\mathbf{n}_k \cdot \nabla\Psi = \frac{1}{c} - \|\nabla\theta_k\| \ , \tag{10}$$

where $\mathbf{n}_k = \nabla\theta_k / \|\nabla\theta_k\|$ is the forward-oriented unit vector normal to the isochrone $\theta_k =$ const. If the local propagation velocity is too fast (*i.e.*, the right hand side is positive), a correction $\theta_{k+1} = \theta_k + \Psi$ is applied so that the normal component of the gradient $\mathbf{n}_k \cdot \nabla\theta_{k+1} = \|\nabla\theta_k\| + \mathbf{n}_k \cdot \nabla\Psi$ is increased, leading to a slower local propagation velocity and thus regularizing the propagation pattern. The diffusion is needed to obtain a unique, smooth solution and the use of complex numbers facilitates the evaluation of the gradient in the presence of 2π jumps.

The parameters c and D need to be specified. On Γ_i, the local wavelength $\lambda = 2\pi c$ should be equal to the length $L_i \approx 6$ mm of the circuit, so c is set to 1 mm/rad. The diffusion coefficient D enforces the stability of the equation. Its value should be of the order of the squared spatial resolution Δx^2 and is set to 1 mm^2. The results are not very sensitive to this choice. With such a small target conduction velocity ($CV = 2\pi c/T = 4$ cm/s for $T = 160$ ms), the local wavelength decreases at each iteration while becoming more uniform. Iterations are stopped when the median of the local wavelength λ reaches a target value obtained from physiological considerations (CV in the tissue $\times$ period of reentry).

E. Mapping from a geometry to another

The problem of transposing the results from a geometry to another is addressed in this subsection. Our method is applied to six patient-specific models of the left atrium. The objective is to create a mapping between two different triangulated surfaces representing the left atrium. This mapping will serve to generate an equivalent phase map in another

geometry.

First, 13 landmark points are selected manually in each left atrial geometry using a graphic user interface. These points (seed points L1 to L13 defined in Krueger *et al.* [19]) indicate the location of veins, valve and appendage. The holes representing the pulmonary veins and the mitral valve are filled with triangles so that the surface becomes homeomorphic to a sphere. Each geometry is then mapped onto a sphere (without folding) using the CALD algorithm [29] implemented in the SPHARM-MAT Matlab toolbox (Li Shen, Indiana University School of Medicine).

The sphere meshes of two geometries are aligned through rigid registration of the 13 landmark points performed by the 'procrustes' matlab function. Non-rigid registration is carried out in spherical coordinates: the differences in latitude and longitude (mesh deformation) are computed for the 13 points and interpolated in the whole mesh by Laplacian interpolation. As a result, the 13 points of the transformed sphere mesh match those of the reference sphere mesh. Nearest neighbor interpolation between these two sphere meshes (transformed and reference mesh) creates a correspondence between the nodes of the two original left atrial meshes, and thus allows to adapt a phase map to another geometry.

F. Initial condition for a monodomain model

From the phase field $\theta = \arg \phi_k$ (whenever $\phi_k = 0$, θ is set to 0), k being the last iteration, an initial condition for the monodomain propagation model is constructed [12]. First, the period of reentry T is estimated based on the effective refractory period of the membrane model used in the monodomain simulation. The phase field $\theta(\mathbf{x})$ is then converted into an activation map $t_{\text{act}}(\mathbf{x})$ by the formula $t_{\text{act}}(\mathbf{x}) = (1 - \theta(\mathbf{x})/2\pi)T$. By construction, this activation map is only defined on the epicardial surface. Nearest-neighbor interpolation is performed to extend the activation map $t_{\text{act}}(\mathbf{x})$ to the entire three-dimensional domain. As a result, PS (two-dimensional) will be transformed into short transmural filaments (three-dimensional). The initial membrane potential is given by $V_0(\mathbf{x}) = V_{\text{paced}}(t_{\text{act}}(\mathbf{x}))$ and the initial membrane state by $\mathbf{s}_0(\mathbf{x}) = \mathbf{s}_{\text{paced}}(t_{\text{act}}(\mathbf{x}))$, where $V_{\text{paced}}(t)$ and $\mathbf{s}_{\text{paced}}(t)$ are the (steady-state) time courses of the membrane potential and state of the midcell in a strand of cells paced at cycle length T at one of its extremity. A monodomain simulation is finally run from this initial condition and the evolution of the number and location of PS is analyzed.

G. Test cases

Our approach was tested in a simplified geometry representing the atrial epicardium by a triangular surface mesh. Two versions, a coarse ($\approx$ 13,800 nodes; for the eikonal-diffusion solver) and a very coarse ($\approx$ 900 nodes; for creating PS distribution), were designed. These surface meshes were generated and processed using Matlab (The MathWorks, Natick, MA) and VRMesh (VirtualGrid, Seattle City, WA). In order to run monodomain simulations in a three-dimensional volumetric model, a cubic mesh ($\approx$ 750,000 nodes, $\Delta x = 0.33$ mm, uniform thickness ≈ 1.6 mm) was created from the surface mesh by identifying grid points within a given distance (one half of the thickness) from the triangular mesh [7, 14]. The coarse atrial surface model lied within the bulk of the 3D model to enable data extrapolation from the surface mesh to the full 3D mesh. Similarly, six triangulated surfaces representing patient-specific left atrial geometries and their corresponding three-dimensional volumetric models were constructed. In addition, a more sophisticated volumetric atrial model was developed. This model includes a fast conduction system (pectinate muscles, terminal crest and Bachmann's bundle) as well as rule-based specification of fiber orientation [19, 30, 31].

III. RESULTS

A. Generation of phase maps

One thousand phase maps were generated on the simplified atrial epicardial surface based on $n = 1$ to 10 PS randomly distributed over the surface (method of Subsect. II C; 100 realizations for each n). An example with $n = 4$ is displayed in Fig. 1. The initial estimate (Fig. 1A) is qualitatively correct, but the isochrones are not regularly spaced. The eikonal-diffusion solver iteratively improves the spacing between isochrones, creates spiral-like curved wavefronts near PS and handles wavefront collision patterns (Fig. 1F).

The regularization effect of the eikonal-diffusion iterations is quantified in Fig. 2. The median $\bar{\lambda} = \text{median}(\lambda)$ and the coefficient of variation ($\text{median}(|\lambda - \bar{\lambda}|/\bar{\lambda})$) of the local wavelength λ (Eq. 6)) is shown for all 1000 phase maps. In the course of the iterations, the median wavelength (and thus the propagation velocity) and the coefficient of variation decrease monotonically. When n is smaller, more iterations are needed to reach a target wavelength. The evolution of the coefficient of variation is not significantly affected by the

number of PS.

As mentioned above, the actual number of PS in the interpolated phase map (ϕ_0) may be larger than the desired number (n) of PS. An example of such case is shown in Fig. 3. These additional PS result from the process of Laplacian interpolation. They may be required to guarantee the existence of a smooth solution with bounded gradient. Then, the eikonal-diffusion solver preserves the number of PS. The average number of additional PS is documented in Table I for different values of n. A proper choice of the topological charges (based on energy minimization) reduces the number of additional PS as compared to a purely random choice (± 1 with probability 1/2). Configurations exist (even with $n = 2$), however, for which no choice of topological charges prevents the creation of additional PS. Although the desired and actual number of PS may differ, they are well correlated (correlation coefficient: 0.94) and the distribution of actual number of PS is sufficiently uniform (see Fig. 4) to allow the generation of a large number of initial conditions (for a monodomain model) with various numbers of functional reentries.

B. Monodomain simulations

Among the 1000 generated phase maps, 100 were selected with an actual number of PS ranging from 1 to 10 (10 phase maps in each case). The corresponding initial conditions for the monodomain equation were constructed (Subsect. II F). Simulations were run for 5 s starting from these initial conditions with parameters $\beta = 2000\ \mathrm{cm}^{-1}$, $C_m = 1\ \mu\mathrm{F/cm}^2$, and $\sigma = 1.5$ mS/cm (isotropic). No significant difference between epicardial and endocardial activations was found by visual inspection. The analysis of PS in epicardial maps is therefore expected to reliably describe the three-dimensional dynamics in this thin-walled model. Figure 5 shows the phase map and the membrane potential map at initial time and after 2 s for different examples with increasing number of PS. In 7 cases with one or two single PS, the reentry self-terminated within 500 ms. In the other cases with a few PS, the evolution was qualitatively consistent with the activation map predicted by the eikonal-diffusion equation (Fig. 5A–C). When more PS were present, the interaction between wavelets eventually led to a more disorganized dynamics (Fig. 5D). With the given conductivity selected to enable the coexistence of up to 10 PS, the wavelength was slightly shorter than in the phase maps.

For the membrane model used, the evolution approximately preserved the number of PS

observed on the epicardial surface. Figure 6 illustrates the correlation between the average number of PS during simulated AF and in the initial condition (correlation coefficient: 0.82). This demonstrates that the 100 simulations widely differ in terms of spatial complexity (from 1 to more than 10 simultaneous reentries). In the time domain, however, the cycle length was found to be similar in all cases (141±1 ms with a spatial dispersion of 7.6±1.5 ms).

C. Patient-specific geometries

To demonstrate how similar dynamics can be simulated on different atrial geometries, six patient-specific models of the left atrium were created. These models differ by their size (left atrial dilation), number of pulmonary veins (4 or 5) and by the possible presence of a common ostium for two veins (Fig. 7B). These geometries (with holes being filled) were projected on a sphere using the method of Subsect. II E. Non-rigid registration provided a mapping to transform a scalar field on a surface into a scalar field on another surface while preserving macro-scale anatomical pathways as identified by the landmark points. This process is illustrated in Fig. 7A. After further regularization using the eikonal-diffusion equation, similar phase maps representing two spirals (one on each side) were obtained on each left atrial geometry (Fig. 7B).

Monodomain simulations were run in corresponding volumetric models of the left atrium, starting from initial conditions generated from these phase maps. Both spirals present in the initial condition were preserved through the evolution. In two cases, two additional PS were created by front-tail interactions.

D. Simulations in more realistic models

Recent atrial models incorporate some form of anisotropy and a fast conducting system [19, 30, 32]. Although the eikonal-diffusion equation can be adapted to take into account anisotropy [12], a phase map computed with the homogeneity and isotropy assumption can also be used to generate an initial condition in a more sophisticated model. As example, the eikonal approach was applied to a patient-specific volumetric model of the atria including fiber orientation and main fast conducting fiber bundles. A phase map with 4 PS was generated on the left atrium using the method of Subsects. II C and II D. The initial condition

was specified in the left atrium using the computed phased map and extended to the entire atria by attributing resting conditions to all the remaining nodes. Conduction properties were set to: $\sigma_l = 4$ mS/cm (longitudinal) and $\sigma_t = 1$ mS/cm (transverse) in the working myocardium, and $\sigma_l = 10$ mS/cm and $\sigma_t = 2$ mS/cm in the fast conducting system.

Figure 8 shows membrane potential maps during the resulting monodomain simulation. While a reentry maintains a disorganized activity in the left atrium (another one is present on the left atrial anterior wall), the right atrium simply follows the pace determined by the left atrium (Fig. 8C). This illustrates how our method can be applied to initiate a fibrillatory activity with different complexity in the right and the left atrium.

IV. DISCUSSION AND CONCLUSIONS

We have developed a tool for automatically creating random fibrillatory initial conditions in thin-walled three-dimensional cardiac propagation model. The complexity of the dynamics can be controlled in terms of number and location of PS. This enables the construction of a library of episodes of simulated fibrillation with varying levels of complexity (Fig. 6). Our approach also facilitates the initiation of a large number of independent simulations in different patient-specific geometries (Fig. 7). Applications of such library include the design and evaluation of ECG or electrogram processing techniques, and the investigation of the success of a therapeutic intervention (e.g. pharmacological) as a function of dynamical complexity.

Although the approach based on PS is conceptually two-dimensional, the method can be applied to three-dimensional models as long as extrapolation through the thickness is relevant, as is the case in the atria. In thicker preparations or in the ventricles, the approach would be limited to the simulation of scroll waves with transmural filaments. In the presence of anisotropy, anatomical structure (e.g. fast conducting bundles), conduction heterogeneity and microstructure, the method is still valuable even though the eikonal model does not take into account these electrophysiological details and thus provide a less accurate initial representation of activation maps (Fig. 8).

Due to the Laplacian interpolation step (Subsect. II D), additional PS were often generated. Over a large number of realizations of random generation of initial conditions, however, the distribution of the number of PS remained relatively uniform (Fig. 4). The range of num-

ber of PS was broader than desired, suggesting to set the number of PS distributed over the surface (n) to a smaller value than the desired maximal number of PS, according to Table I. An appropriate choice of the topological charges based on the distance between the PS reduced the observed discrepancy (Table I).

Davidsen *et al.* demonstrated that in an oriented, compact, possibly punctured two-dimensional differentiable manifold, the sum of the topological charges of all phase singularities and holes is always zero [7]. If necessary, Laplacian interpolation automatically creates additional topological charges to satisfy this conservation law. For instance, when n is odd, either a new PS is created or an additional topological charge is placed in a hole. When n is even, additional PS may also be created due to geometrical constraints or distribution of charge, as illustrated by Fig. 3. In this case, Laplacian interpolation creates two PS of opposite charges (or one PS and a topological charge in a hole) to satisfy the conservation law.

The eikonal-based regularization of the phase map (Subsect. II D) requires three parameters: c, D and λ. In previous works, the velocity c and the diffusion parameter D were selected to reproduce activation maps computed using a monodomain model [12]. Here, the eikonal-diffusion equation serves solely to regularize the phase map and reduce spatial variations in propagation velocity. Generated phase maps are not expected to match those obtained during multiple-reentry dynamics since the eikonal-diffusion equation lacks any information about repolarization [24]. Its purpose is only to provide a sufficiently relevant approximation for the phase map so that the simulated evolution may preserve the complexity of the dynamics (Fig. 6). In this context, c is set to a small value to allow high-curvature fronts and D is set to a mesh-related value to guarantee the stability of the algorithm [13]. A larger c would be incompatible with the presence of the PS (uniform conduction properties are assumed). With these parameters, the target wavelength is very short in such a way that the solution exists close to the PS. Iterations are stopped when the wavelength is uniform enough and has a realistic mean value λ (Fig. 2). An alternative approach would be to reduce propagation velocity (in the eikonal equation) in the vicinity of each PS in order to mimic conduction velocity restitution and ensure convergence of the iterations. This would require more parameter adjustment without necessarily generating more realistic phase maps.

Once an initial condition is created, its evolution and spiral dynamics strongly depend on membrane properties, for instance action potential duration restitution [36]. We chose mem-

brane properties to allow the coexistence of multiple PS with limited meandering, leading to a relatively stable number of PS. Faster conduction velocity or longer action potentials would have resulted in the disappearance of most of the PS. Ionic heterogeneities would have created a substrate for increased wavebreak occurrence. Our eikonal approach is not intended to incorporate these effects. Instead, it provides a tool for investigating these phenomena under a wider range of controlled (initial) conditions and a larger number of its statistical realizations.

ACKNOWLEDGMENTS

The authors thank Alain Vinet (Université de Montréal, Canada) for helpful discussions and comments, the Lausanne Heart Group (Ecole Polytechnique Fédérale de Lausanne, Switzerland) for sharing simulation tools and Lam Dang and Christoph Scharf (HerzGefässZentrum, Klinik im Park, Zurich, Switzerland) for providing geometrical data to create patient-specific models.

This work was supported by funding from the Natural Sciences and Engineering Research Council of Canada, Heart & Stroke Foundation of Québec and Fonds de Recherche en Santé du Québec.

---

[1] Buzzard, G. T., J. J. Fox, and F. Siso-Nadal, 2008, SIAM J Sci Comput **30**, 837.

[2] Clayton, R. H., E. A. Zhuchkova, and A. V. Panfilov, 2006, Prog Biophys Mol Biol **90**(1-3), 378.

[3] Cormen, T. H., C. E. Leiserson, R. L. Rivest, and C. Stein, 2001, *Introduction to Algorithms* (MIT Press).

[4] Courtemanche, M., R. J. Ramirez, and S. Nattel, 1998, Am J Physiol **275**(1 Pt 2), H301.

[5] van Dam, P. M., and A. van Oosterom, 2003, J Cardiovasc Electrophysiol **14**(10 Suppl), S166.

[6] Dang, L., N. Virag, Z. Ihara, V. Jacquemet, J. M. Vesin, J. Schlaepfer, P. Ruchat, and L. Kappenberger, 2005, Ann Biomed Eng **33**(4), 465.

[7] Davidsen, J., L. Glass, and R. Kapral, 2004, Phys Rev E Stat Nonlin Soft Matter Phys **70**(5 Pt 2), 056203.

[8] Dobrev, D., E. Wettwer, A. Kortner, M. Knaut, S. Schuler, and U. Ravens, 2002, Cardiovasc Res **54**(2), 397.

[9] Gong, Y., F. Xie, K. M. Stein, A. Garfinkel, C. A. Culianu, B. B. Lerman, and D. J. Christini, 2007, Circulation **115**(16), 2094.

[10] Haissaguerre, M., K. T. Lim, V. Jacquemet, M. Rotter, L. Dang, M. Hocini, S. Matsuo, S. Knecht, P. Jais, and N. Virag, 2007, Europace **9 Suppl 6**, vi64.

[11] Iyer, A. N., and R. A. Gray, 2001, Ann Biomed Eng **29**(1), 47.

[12] Jacquemet, V., 2010, IEEE Trans Biomed Eng **57**(9), 2090.

[13] Jacquemet, V., 2011, Comput Methods Programs Biomed (in press).

[14] Jacquemet, V., A. van Oosterom, J. M. Vesin, and L. Kappenberger, 2006, IEEE Eng Med Biol Mag **25**(6), 79.

[15] Jacquemet, V., N. Virag, Z. Ihara, L. Dang, O. Blanc, S. Zozor, J. M. Vesin, L. Kappenberger, and C. Henriquez, 2003, J Cardiovasc Electrophysiol **14**(10 Suppl), S172.

[16] Kharche, S., G. Seemann, J. Leng, A. Holden, C. Garratt, and H. Zhang, 2007, in *Proceedings of the 4th international conference on Functional imaging and modeling of the heart* (Springer-Verlag), pp. 129–138.

[17] Kneller, J., J. Kalifa, R. Zou, A. V. Zaitsev, M. Warren, O. Berenfeld, E. J. Vigmond, L. J. Leon, S. Nattel, and J. Jalife, 2005, Circ Res **96**(5), e35.

[18] Kneller, J., R. Zou, E. J. Vigmond, Z. Wang, L. J. Leon, and S. Nattel, 2002, Circ Res **90**(9), E73.

[19] Krueger, M., V. Schmidt, C. Tobón, F. Weber, C. Lorenz, D. Keller, H. Barschdorf, M. Burdumy, P. Neher, G. Plank, *et al.*, 2011, in *Functional Imaging and Modeling of the Heart* (Springer), pp. 223–232.

[20] Lemay, M., Y. Prudat, V. Jacquemet, and J. M. Vesin, 2008, IEEE Trans Biomed Eng **55**(11), 2538.

[21] Lemay, M., J. M. Vesin, A. van Oosterom, V. Jacquemet, and L. Kappenberger, 2007, IEEE Trans Biomed Eng **54**(3), 542.

[22] Nattel, S., A. Maguy, S. Le Bouter, and Y.-H. Yeh, 2007, Physiol Rev **87**(2), 425.

[23] Oostendorp, T., A. van Oosterom, and G. Huiskamp, 1989, J Comput Phys **80**(2), 331.

[24] Pernod, E., M. Sermesant, E. Konukoglu, J. Relan, H. Delingette, and N. Ayache, 2011, Computers & Graphics **35**(2), 431.

[25] Plonsey, R., and R. C. Barr, 2000, *Bioelectricity: A Quantitative Approach* (Kluwer Academic Plenum Publishers).

[26] Qu, Z., and J. N. Weiss, 2005, Am J Physiol Heart Circ Physiol **289**(4), H1692.

[27] Reumann, M., J. Bohnert, G. Seemann, B. Osswald, and O. Dossel, 2008, IEEE Trans Biomed Eng **55**(2 Pt 1), 399.

[28] Ruchat, P., L. Dang, J. Schlaepfer, N. Virag, L. K. von Segesser, and L. Kappenberger, 2007, Eur J Cardiothorac Surg **32**(1), 90.

[29] Shen, L., and F. Makedon, 2006, Image Vision Comput **24**(7), 743.

[30] Tobon, C., C. Ruiz, J. F. Rodriguez, F. Hornero, J. M. Ferrero, and J. Saiz, 2010, Conf Proc IEEE Eng Med Biol Soc **2010**, 224.

[31] Vigmond, E. J., R. Ruckdeschel, and N. Trayanova, 2001, J Cardiovasc Electrophysiol **12**(9), 1046.

[32] Vigmond, E. J., V. Tsoi, S. Kuo, H. Arevalo, J. Kneller, S. Nattel, and N. Trayanova, 2004, Heart Rhythm **1**(3), 334.

[33] Virag, N., V. Jacquemet, C. S. Henriquez, S. Zozor, O. Blanc, J. M. Vesin, E. Pruvot, and L. Kappenberger, 2002, Chaos **12**(3), 754.

[34] Weber, F. M., C. Schilling, G. Seemann, A. Luik, C. Schmitt, C. Lorenz, and O. Dossel, 2010, IEEE Trans Biomed Eng **57**(10), 2394.

[35] Workman, A. J., K. A. Kane, and A. C. Rankin, 2001, Cardiovasc Res **52**(2), 226.

[36] Xie, F., Z. Qu, A. Garfinkel, and J. N. Weiss, 2002, Am J Physiol Heart Circ Physiol **283**(1), H448.

Table I. Number of additional phase singularities (PS) for different values of the desired number (n) of PS using the energy-based (minimizing Eq. (5)) or purely random choice of topological charges. Mean and standard deviation over 100 phase maps are reported.

	#additional PS	
n	energy-based	random sign
1	0.4 ± 0.5	0.4 ± 0.5
2	1.0 ± 0.7	1.0 ± 0.7
3	1.2 ± 0.7	1.4 ± 0.7
4	1.7 ± 0.9	1.8 ± 0.8
5	2.0 ± 1.0	2.4 ± 1.0
6	2.1 ± 1.1	2.7 ± 1.1
7	2.5 ± 1.2	3.3 ± 1.1
8	3.1 ± 1.2	4.0 ± 1.2
9	3.2 ± 1.4	4.7 ± 1.4
10	3.6 ± 1.4	5.1 ± 1.5

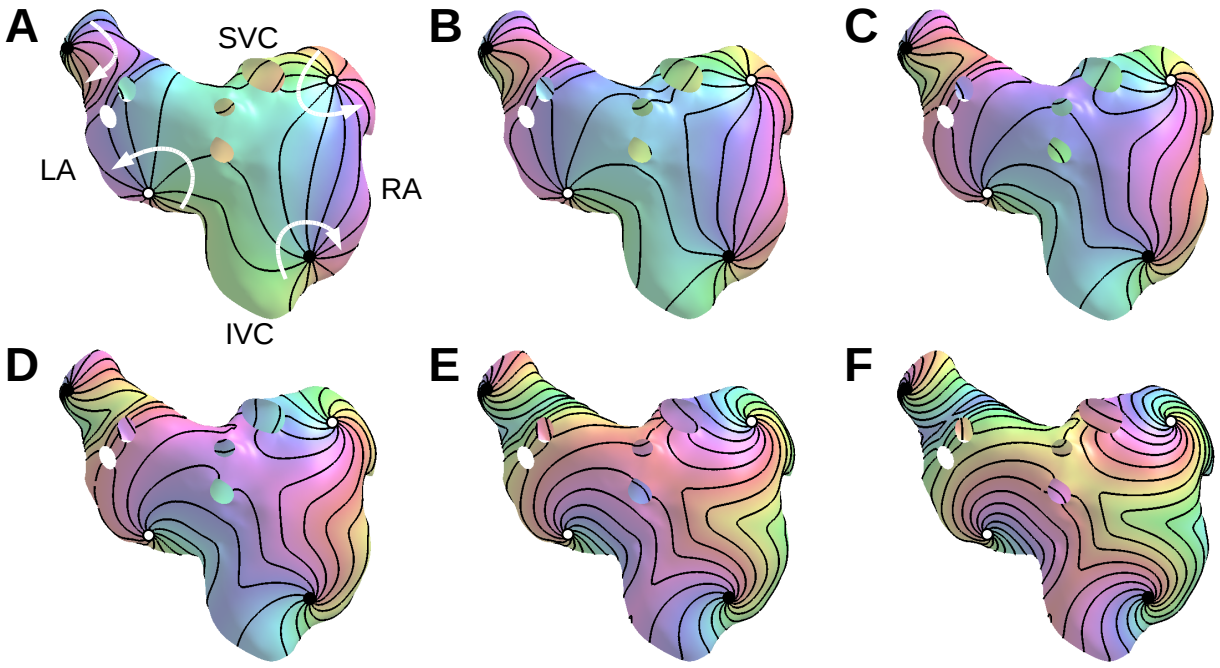

Figure 1. Phase maps generated from four phase singularities (PS). PS with positive/negative topological charge are shown as a white/black circle. White arrows illustrate the direction of propagation. Solid lines represent ten isochrones regularly distributed between 0 and 2π. (A) initial phase map ϕ_0 obtained by Laplacian interpolation; (B)–(E) phase map after 10, 20, 30, 50 iterations of the eikonal-diffusion solver; (F) final phase map (after 68 iterations, the target wavelength of 6 cm is reached). LA: left atrium; RA: right atrium; SVC: superior vena cava; IVC: inferior vena cava.

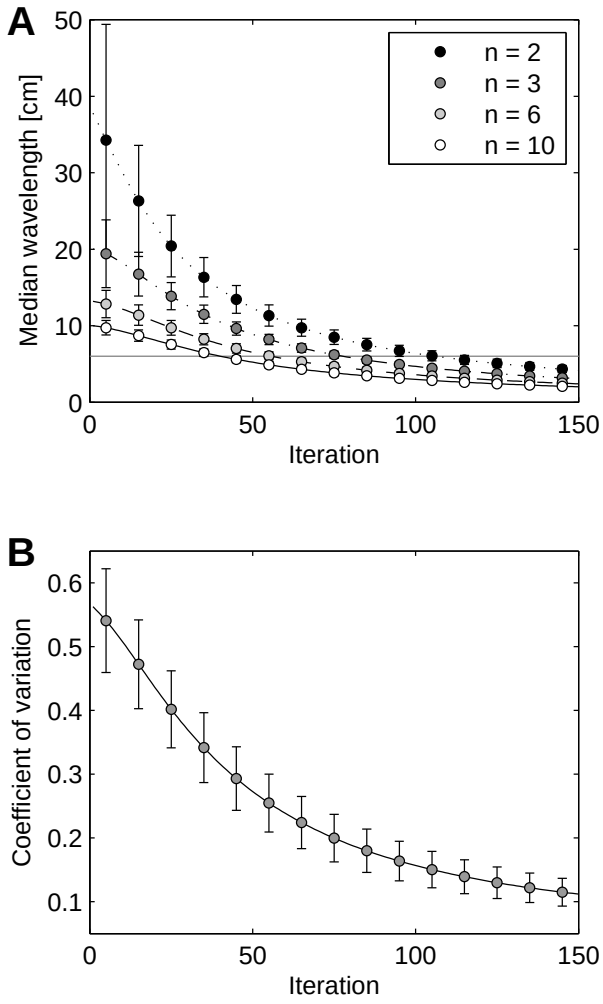

Figure 2. Regularization of phase maps using eikonal-diffusion iterations. (A) Median wavelength λ (spatial average of Eq. (6)) throughout the iterations for $n = 2, 3, 6$ and 10 initial phase singularities. Mean and standard deviation over 100 phase maps are displayed. The horizontal line indicates the target wavelength $\lambda = 6$ cm. (B) Coefficient of variation of the wavelength λ throughout the iterations (pooled data for $n = 1$ to 10). Mean and standard deviation over 1000 phase maps are displayed.

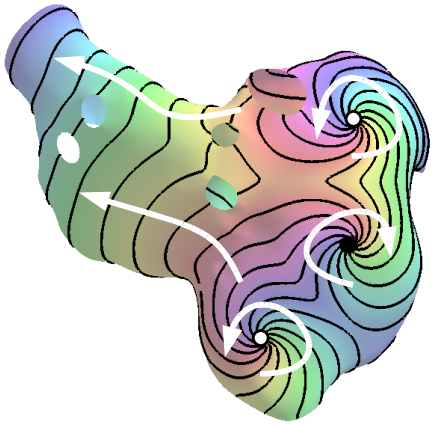

Figure 3. Example of phase map generated from two phase singularities (PS) with the same positive topological charge (white circle). An additional PS with opposite topological charge (black circle) is created by the Laplacian interpolation procedure between the two original ones. White arrows illustrate the direction of propagation. Solid lines represent ten isochrones regularly distributed between 0 and 2π.

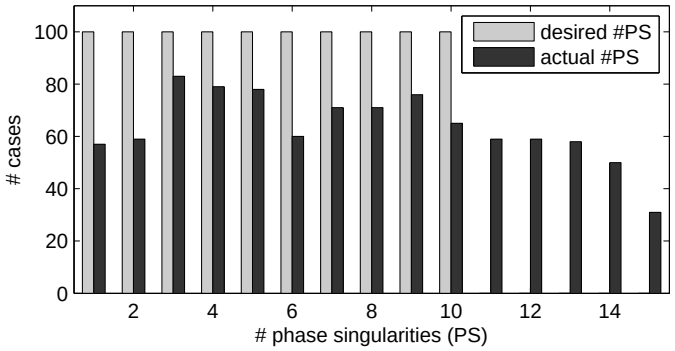

Figure 4. Histogram of desired (n) and actual number of phase singularities (as measured in the phase maps resulting from the eikonal-diffusion solver). The total number of phase maps generated is 1000.

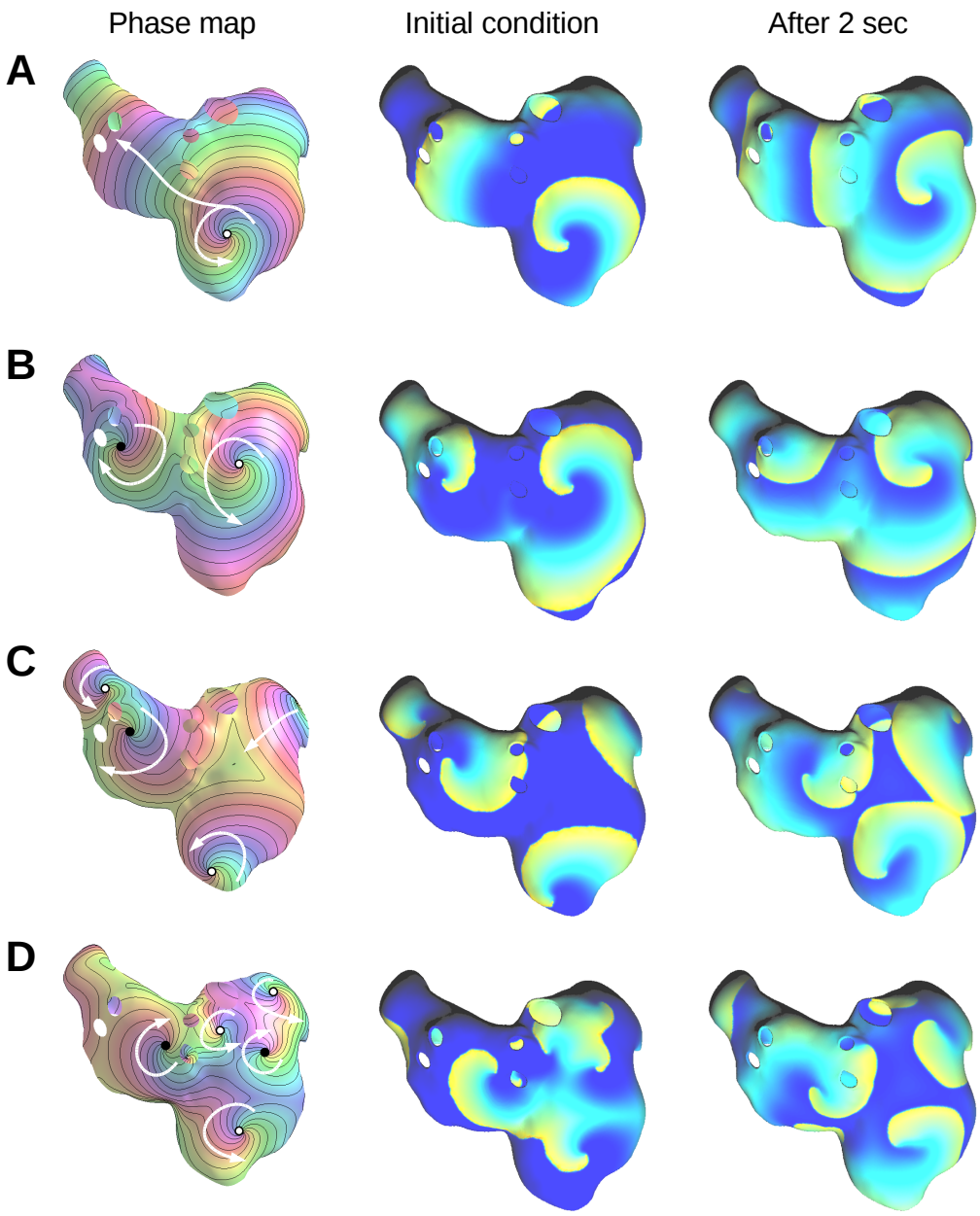

Figure 5. Examples of phase maps reconstructed using the eikonal-diffusion equation (first column) and membrane potential maps at initial time (second column) and after 2 s of simulation (third column). Phase singularities with positive/negative topological charge are shown as a white/black circle. White arrows illustrate the direction of propagation. Solid lines represent twelve isochrones regularly distributed between 0 and 2π. Membrane potential maps are color-coded from blue (-80 mV) to yellow (20 mV).

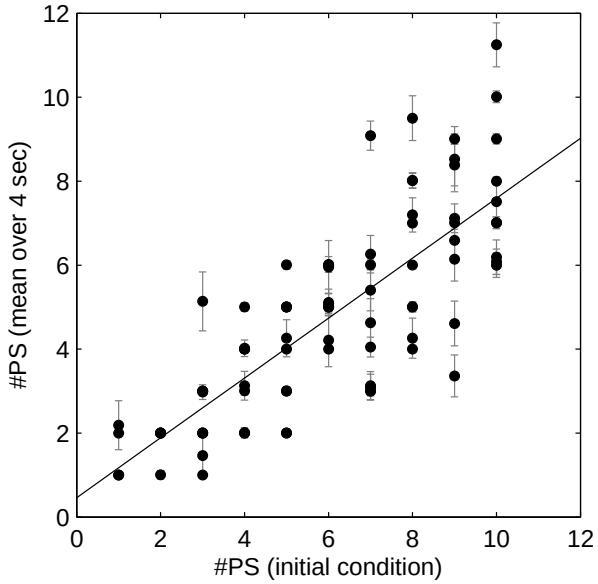

Figure 6. Time-averaged number of phase singularities (PS) during simulated AF (mean from $t = 1$ s to $t = 5$ s for each simulation; standard deviation over the same time interval shown as error bars) as a function of the number of PS in the initial condition. Note that several data points may be superimposed. Linear regression curve is displayed.

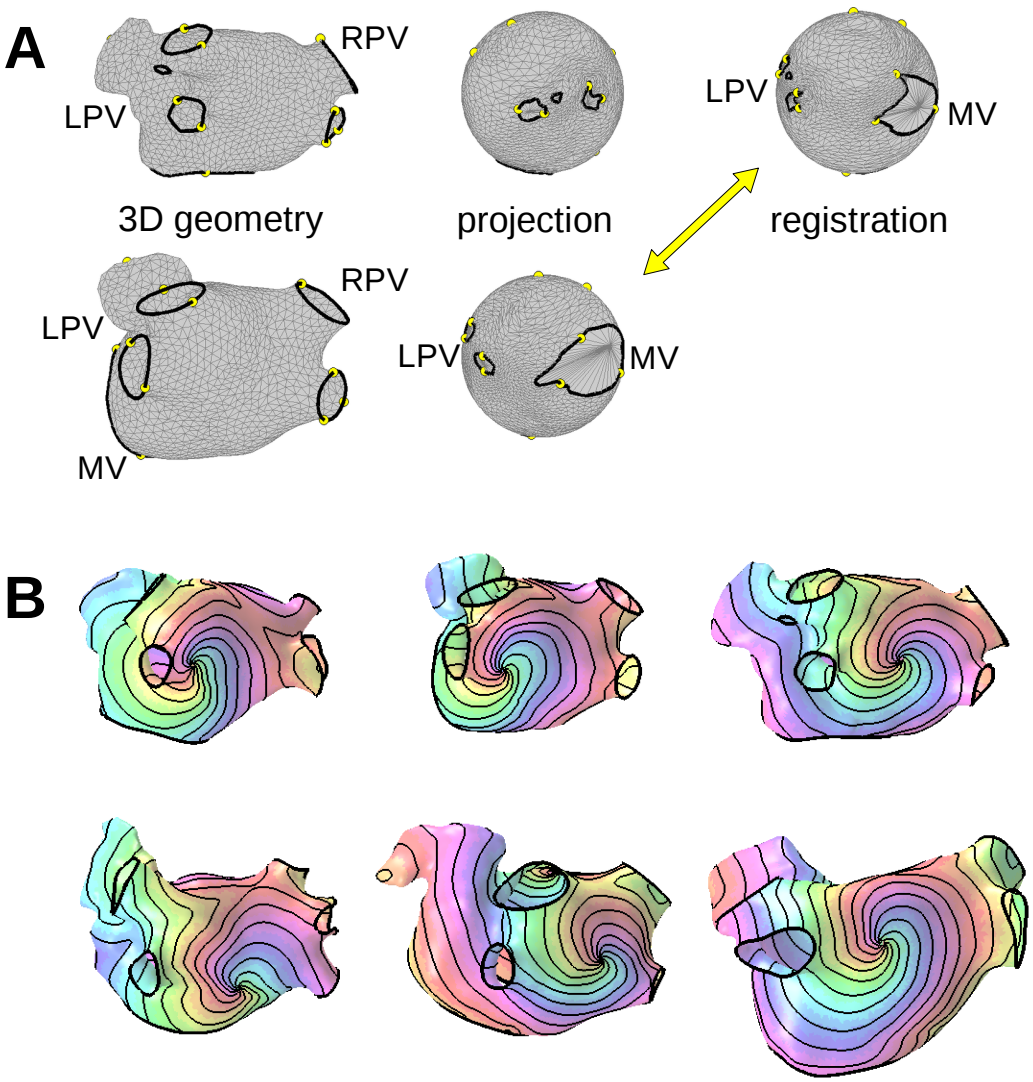

Figure 7. Transfer from a geometry to another. (A) Two geometries of the left atrium and their projection on the sphere are displayed. Coarse versions of the meshes are used for visualization in this figure. The top-right sphere is obtained after non-rigid registration. The dots represent the location of the 13 landmark points on each surface. Valve and veins are shown as thick black lines. LPV: left pulmonary veins; RPV: right pulmonary veins; MV: mitral valve. (B) Six examples of phase maps transferred from the third one on the first row (after eikonal-based regularization). Solid lines represent ten isochrones regularly distributed between 0 and 2π.

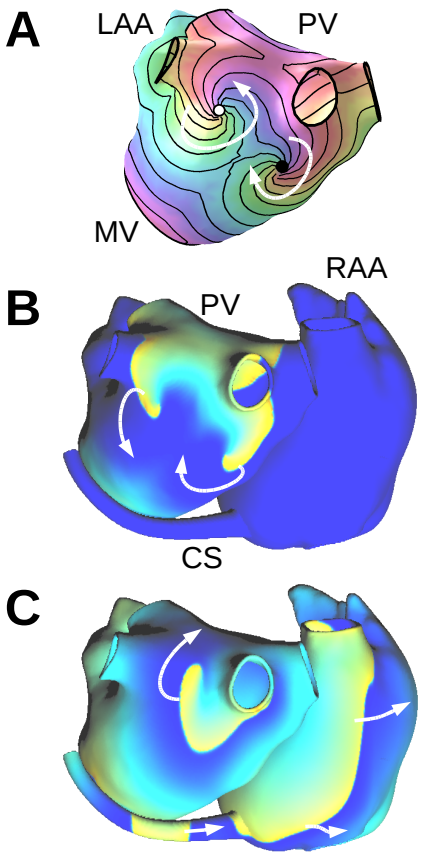

Figure 8. Initiation of reentries in a three-dimensional model with fiber orientation and fast conducting bundles. (A) Phase map generated using the eikonal-diffusion approach in the left atrium (posterior view); ten isochrones regularly distributed between 0 and 2π are shown as solid lines. (B) Membrane potential map representing the initial condition in the monodomain model (posterior view); membrane potential maps are color-coded from blue (-80 mV) to yellow (20 mV). (C) Membrane potential map at time $t = 600$ ms. PV: pulmonary veins; LAA: left atrium appendage; MV: mitral valve; RAA: right atrium appendage; CS: coronary sinus.